








USE OF AIRBORNE GEOPHYSICS FOR POTENTIAL Fe-Ti-V OXIDES MINERALIZATION IN METAGABBROS: AN EXAMPLE WITHIN THE PALEOPROTEROZOIC BASEMENT OF RIBEIRA BELT, SOUTHEAST BRAZIL

Ana Caroline D. Dutra ^{1,2,3*}, Suze Nei P. Guimarães ⁴, Marcelo dos Santos Salomão ^{3,5}, Nely Palermo ⁵, Luís Carlos Bertolino ⁶, Henrique Bruno ⁵, and Miguel Angelo Mane ²

¹ Universidade do Estado do Rio de Janeiro - UERJ, PPGG - Programa de Pós-Graduação em Geociências, Faculdade de Geologia, Rio de Janeiro, RJ, Brazil

² Universidade do Estado do Rio de Janeiro - UERJ, LAGEX - Laboratório de Geofísica Exploratória, Faculdade de Geologia, Departamento de Geologia Aplicada, Rio de Janeiro, RJ, Brazil

³ Universidade do Estado do Rio de Janeiro - UERJ, LEXMIN - Laboratório de Exploração Mineral, Faculdade de Geologia, Departamento de Geologia Aplicada, Rio de Janeiro, RJ, Brazil

⁴ Observatório Nacional - ON, Laboratório de Geotermia, Rio de Janeiro, RJ, Brazil

⁵ Universidade do Estado do Rio de Janeiro - UERJ, TEKTOS - Grupo de Pesquisa em Geotectônica, Faculdade de Geologia, Departamento de Geologia Regional e Geotectônica, Rio de Janeiro, RJ, Brazil

⁶ Centro de Tecnologia Mineral - CETEM, Rio de Janeiro, RJ, Brazil

*Corresponding author email: geoanacaroline@gmail.com

ABSTRACT. The use of aerogeophysics applied to mineral exploration constitutes an important tool in investigation of metalliferous deposits. In this sense, the present study was motivated by a 720-ppm vanadium anomaly, associated with metagabbroic rocks inserted in the context of the Paleoproterozoic basement of the Ribeira Belt, south of Minas Gerais state, Brazil. This work aims to characterize metagabbros with potential for Fe-Ti-V oxides, through the integration of geological and geophysical data. As a result of the fieldwork, a lithostratigraphic zoning was proposed to characterize contact relationships of the metagabbro with the enclosing rocks, where the main zone marks the presence of the metagabbro garnet, considered a target of a prospective campaign for investigation of the ore. Subsequently, geological data were correlated to magnetic and radiometric images, resulting in a new geological map that shows the arrangement of metagabbroic bodies and structural aspects. In addition, it provides subsidies for the selection of potential enrichment areas for minerals carrying vanadium, magnetite, and ilmenite. The correlations between geology and geophysics were quite coherent, helping to understand the structure, local geology, and distribution of the metagabbro garnet, considered a prospective guide for mineralization of Fe-Ti-V oxides in the research area.

Keywords: integrated geophysical methods; anomaly; vanadium; magnetometry; radiometry.

INTRODUCTION

Aerogeophysical survey is commonly used in geological mapping and mineral exploration (Sharma, 1987), especially in identification and delimitation of metalliferous deposits (Maas et al., 2003; Carrino et al., 2007; Gaafar, 2015). The geophysical methods of magnetometry and radiometry allow the investigation of geological structures in subsurface and compositional variations of these rocks by different magnetic response

and distribution of natural radioelements (K-U-Th), configuring physical contrasts in the property evaluation of these lithotypes (Telford et al., 1990; Minty, 1997).

Scientific and technological development allowed advances in the accuracy and resolution of geophysics to better characterize geological and structural aspects of a region. In this context, the studies developed by Carvalho et al. (2006), Carneiro and Barbosa (2008), Ferraz et al. (2008), and Guimarães and Hamza (2009) used magnetic

data to assist the geological mapping and characterization of structural guidelines. Similarly, [Maas et al. \(2003\)](#), [Ortiz Suárez et al. \(2012\)](#), and [Pereira et al. \(2016\)](#) applied the magnetometric method to the study of areas with potential mineralization for iron oxides, gold, copper, and platinum group elements.

The studies accomplished in this research were motivated by the results of [Pinto \(1995\)](#), who carried out a chemical analysis campaign in the region, with one of the geochemical acquisition points presenting 720 ppm of vanadium, awakening the area to an investigation for mineral prospecting. The vanadium anomaly is related to basic rocks associated with the Archean/Paleoproterozoic Piedade Block ([Bruno et al., 2020, 2021](#)), considered the basement of Andrelândia Domain belonging to the Neoproterozoic Ribeira Belt ([Heilbron et al. 2000, 2004; Tubinambá et al., 2007](#)) illustrated in [Figure 1](#). The geology of the study area comprises a set of tholeiitic metabasic rocks, named by [Viana \(1991\)](#) as São Bento dos Torres Suite, and by [Hiraga et al. \(2017\)](#) as the Oliveira Fortes unit, within the context of the Archean/Paleoproterozoic Piedade block ([Figure 2](#)). The latter is characterized by a lithological association that includes biotite leucogneisses, (hornblende)-biotite gneiss, tonalite-thronthjemite-granodiorite (TTG), sanukitoid and high-K granitoids, whose ages range from the Archean to the Paleoproterozoic, and records a complete orogenic cycle of subduction, collision, and collapse during the Minas-Bahia orogenic cycle ([Hiraga et al., 2017; Bruno et al., 2020, 2021](#)).

In the Aracitaba region (southern Minas Gerais), the anomalous concentration of vanadium is associated with the garnet-rich metagabbro, characterized by [Pinto \(1995\)](#). These rocks have gabbroic composition, and they are gray to greenish colored and fine to medium grained. They present subophytic textures in a relic character and polygonal and coronitic textures, with metamorphic conditions in amphibolite facies, with local records of granulite facies according to [Hiraga et al. \(2017\)](#). Lithochemical data from these rock show vanadium concentrations above 480 ppm, associated with an enrichment of light rare Earth elements (LREE) ([Table 1](#)).

Considering that vanadium occurs in the upper crust with an abundance of approximately 60 ppm ([Taylor and McLennan, 1995](#)) and a background of around 250 ppm in mafic rocks ([Kelley et al., 2017](#)), the content found in the Aracitaba region was considered anomalous in terms of vanadium, being then responsible for instigating this research, in an approach linked to geophysical exploration. Within this context, the present work aims

to correlate areas favorable to the occurrence of gabbroic bodies, the main metalotect for Fe-Ti-V mineralization in Aracitaba, using the aerogeophysical survey of the Minas Gerais state (Program 2010/2011) to assist in geological mapping aimed at the prospective vanadium campaign.

MATERIALS AND METHODS

The activities conducted in this study included the processing of airborne geophysical data, and the mapping and characterization of mafic rocks through petrography. The data used in the study are part of the airborne survey of the Area 15 (Juiz de Fora, Cataguases and Manhuaçu) and were provided by CODEMIG (Company of Economic Development of Minas Gerais) to the Geology Department of the Rio de Janeiro State University (UERJ).

The parameters that guided the execution of this airborne survey were year of acquisition between 2010 and 2011, lines with N-S direction, lines with a spacing of 500 m, tie line with E-W direction, tie line with a spacing of 10.000 m, flight height of 100 m, approximate flight speed of 280 km/h and about 76.500 km of profiles. The data are interpreted, including modeling of geophysical data and elaboration of magnetic and radiometric maps, using the Oasis Montaj 8.4 software (Geosoft S.A. / Seequent) to integrate with the geological interpretation of the study area ([Figure 3](#)).

Anomalies in the Earth's magnetic field are influenced by the variation in the rate of magnetic minerals in the composition of subsurface rocks. In this way, studies involving the anomalous magnetic field are used to investigate subsurface structures, offering information such as geometry and depth of their sources. In addition to identifying the sources, through the processing of these magnetic data, it is possible to delineate and map folds, faults and other structures.

The removal of the International Geomagnetic Reference Field (IGRF) was applied to the airborne magnetic data, resulting in a channel in the database referring to the crustal magnetic anomalies. The bidirectional interpolation method ([Whitehead, 2010](#)) was used in these data with a cell at a quarter of the spacing between the flight lines (125 X 125 m), following the Nyquist criterion ([Davis, 1986](#)). This method is widely applied to data acquired in an oriented way because is inherent to this interpolator used to reinforce trends perpendicular to the direction of the flight line, reducing the presence of noise in the data. The resulting grid represents the anomalous magnetic field (AMF).

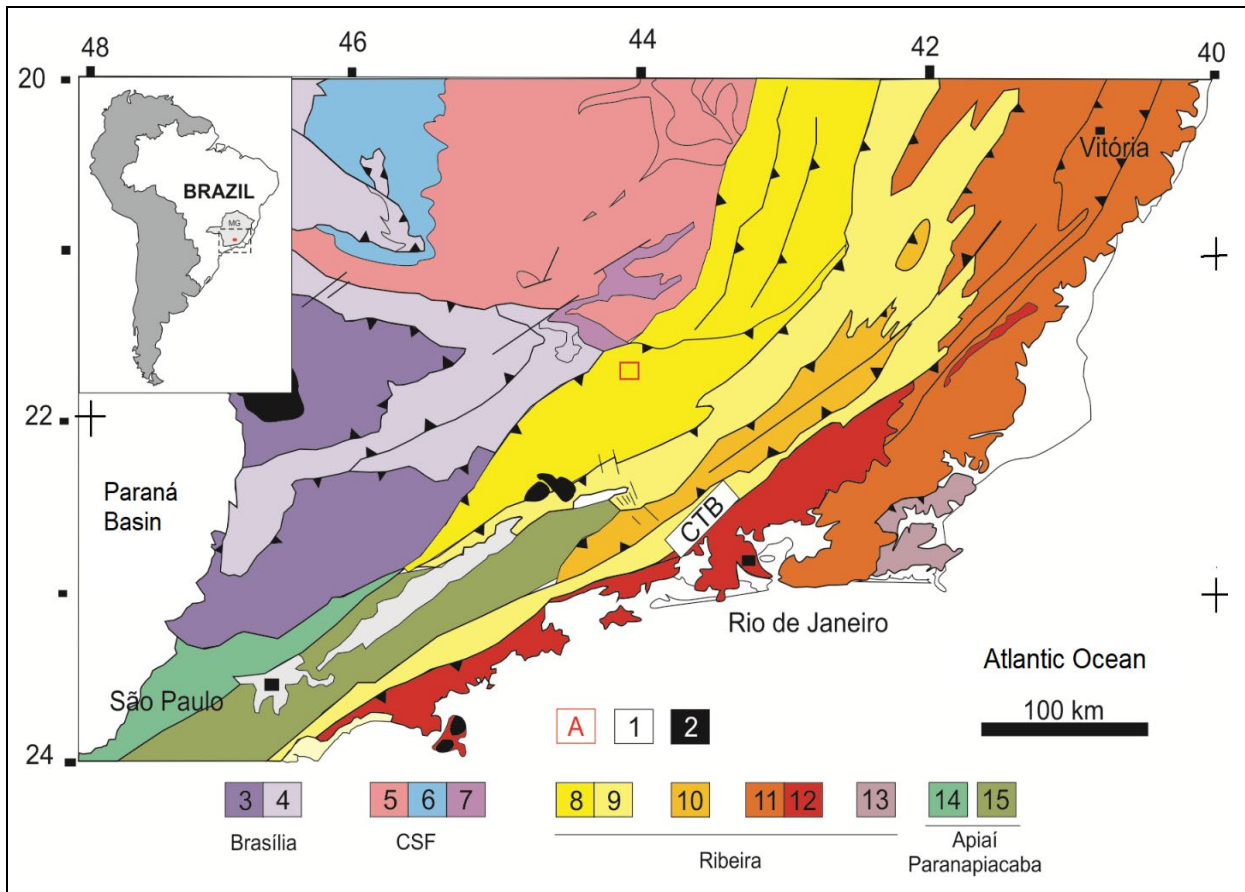


Figure 1: A geological map of Southeast Brazil showing the tectonic compartment of the Ribeira Belt (adapted from [Tupinambá et al., 2007](#)). The major blocks shown in the inset are: **A**- Study area; **1**- Cenozoic Rifts; **2**- Cretaceous and Tertiary alkaline rocks; **3**- Inferior Nappes; **4**- Superior Nappes; **5**- Basement and Autochthonous domain; **6**- San Francisco Supergroup; **7**- Metasediments of the Autochthonous domain; **8**- Andrelândia domain; **9**- Juiz de Fora domain of the Occidental terrain; **10**- Paraíba do Sul Klippe; **11**- Oriental terrain; **12**- Granitoids of the Rio Negro magmatic arc; **13**- Cabo Frio terrain; **14**- São Roque and Açungú terrains; **15**- Embu terrain.

Table 1: Vanadium content associated with the basic granulite of the São Bento dos Torres Suite.

ID	Host lithotype	Vanadium content
1	Pyriboleite (Population 2)	510 ppm
2	Pyriclasite (Population 1)	490 ppm
3	Pyriboleite (Population 2)	480 ppm
4	Pyriboleite (Population 2)	720 ppm
5	Pyriclasite (Population 1)	310 ppm
6	Pyriclasite (Population 3)	370 ppm
7	Pyriclasite (Population 3)	380 ppm

Adapted from [Pinto \(1995\)](#).

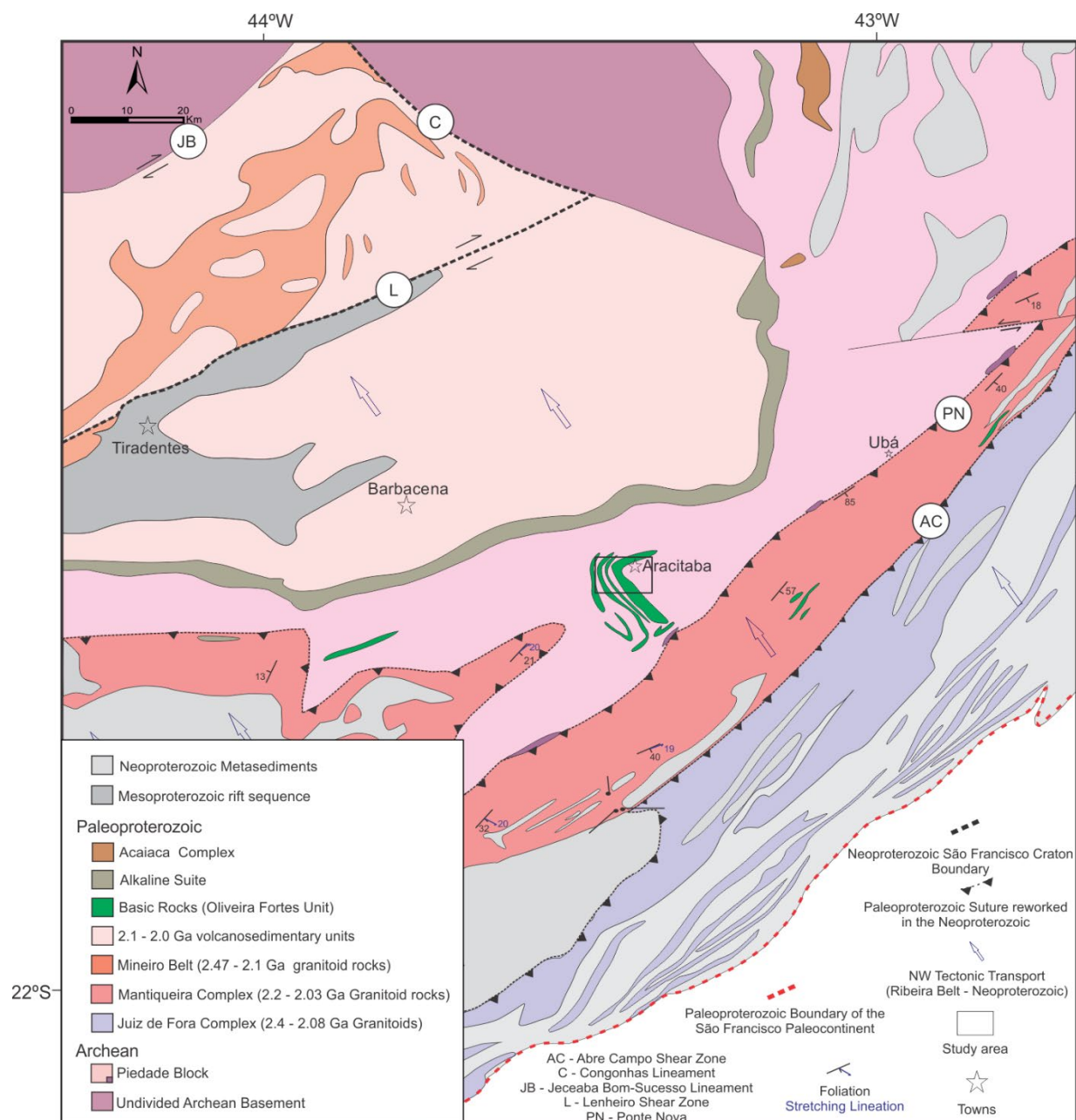


Figure 2: Location of the study area (black polygon). Adapted from [Bruno et al. \(2020\)](#).

From this AMF grid some geophysical interpretation techniques (filtering) were applied to the following contour maps, such as vertical derivative ([Gunn, 1975](#)), analytic signal amplitude (ASA) ([Nabighian, 1972](#)) and analytical signal inclination (ISA) or Tilt derivative (TILT) ([Miller and Singh, 1994](#)), to obtain a spatial investigation about magnetic anomalous sources.

The grids of the radiometric data were interpolated by the minimum curvature method ([Briggs, 1974](#)), using a regular 125m spacing, to obtain the radioelement concentration maps (potassium - K, thorium - Th and uranium - U) and the ternary composition map (standard red, green and blue colors - RGB). For the geological mapping of the area, a georeferenced base in ArcGIS was

created, integrating the following products: a 1:50,000 topographical map of Folha Paiva ([IBGE, 1976](#)), a geological map of Folha Rio Pomba in the scale of 1:100,000 ([Brandalise and Viana, 1993](#)), and a geological map of the Minas Gerais state (1:1,000,000). The field activities aimed at the regional geological recognition. Then, it was made a geological mapping, in a local scale, of outcropping gabbroic bodies and host lithotypes, including description, sampling, and obtaining measures of magnetic susceptibility.

Magnetic susceptibility (MS) measurements were obtained using an Exploranium susceptibility meter (model Kappameter KT-9), which detects the MS of materials in a range between 1×10^{-5} and 999×10^{-3} (SI).

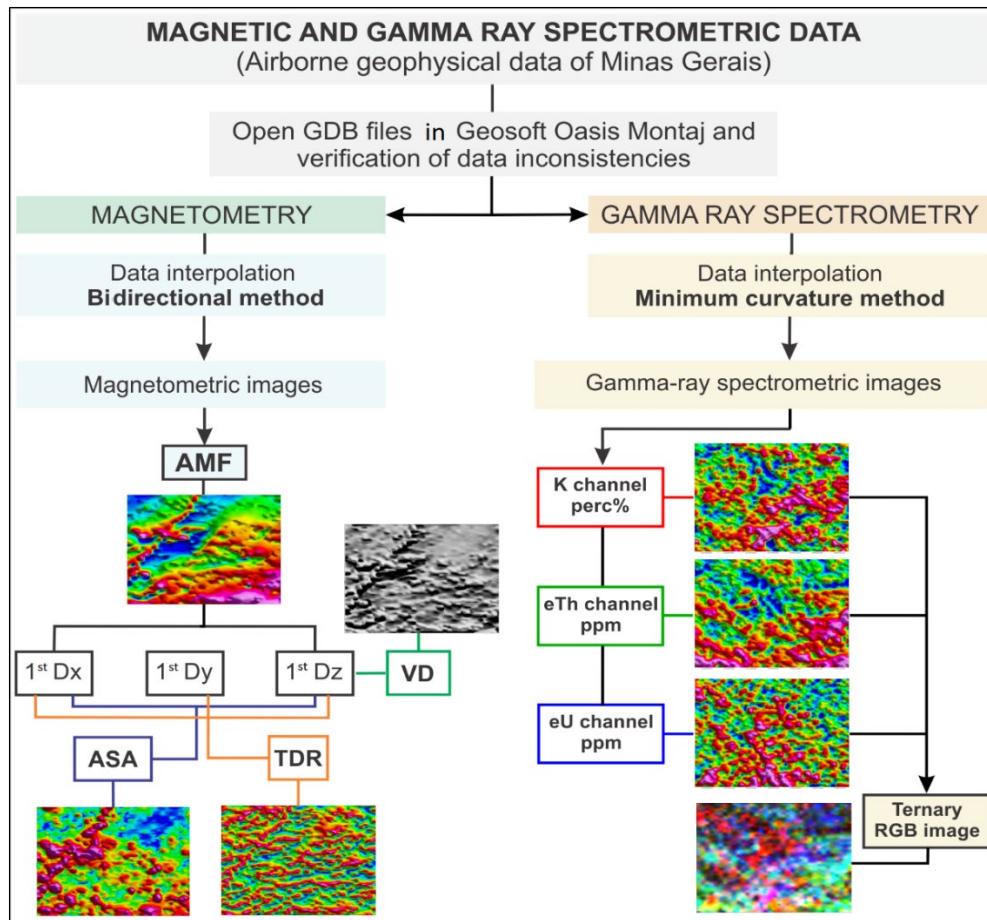


Figure 3: Flowchart showing techniques used for the treatment of aerogeophysical data.

The equipment was used in the outcrops of metagabbros during the fieldwork, and in the laboratory, on hand samples. The objective was to identify the presence of magnetite, a mineral that may contain vanadium in its composition. Outcrops with a high-level of weathering were avoided. Ten susceptibility readings were performed on each sample to obtain an average of the magnetic susceptibility for the rock.

RESULTS

Local Geology

Based on the distribution of the lithotypes and on the structural aspects found around the vanadium anomaly, a lithostratigraphic column consisting of three zones was defined (Figure 4). The lower zone (LZ) is predominantly formed by (hornblende) biotite gneiss with thin layers and lenses of mafic rocks. In the basal portion of the LZ, the biotite gneiss is white, fine-grained, and has mylonitic features, which refer to regional shear zones. The outcrops are, in general, quite weathered, which reflects on the friable aspect of the rock. Locally, pockets of quartz-feldspathic composition

with mafic enclaves can be observed, suggesting a punctual partial melting process (Figure 4A). Granulites occur in an isolated region, as rock blocks or thin layers interspersed with (hornblende) biotite gneiss, reaching a high magnetic susceptibility. Despite sparse outcrops, in the intermediate portion of the zone, parasitic folds (Figure 4B) and intrafolial folds (Figure 4C) are found in weathered road sections. Lens foliated metagabbros become more recurrent when near the top of the LZ, where they present up to one meter thick, and are irregularly distributed and without lateral continuity along the LZ (Figure 4D), indicating an increase in the presence of mafic rocks.

The main zone (MZ) is characterized by the presence of metamorphosed gabbroic bodies, called garnet-metagabbro. Three main gabbroic bodies were individualized. The most representative body outcrops in an old quarry (Figure 4E), extracted for ornamental purposes and is approximately 20-meter high. This body is located between two thinner layers of metagabbro (approx. 4 meters) and has a marked foliation and a high degree of alteration. The garnet-metagabbro corresponds to the lithotype targeted by

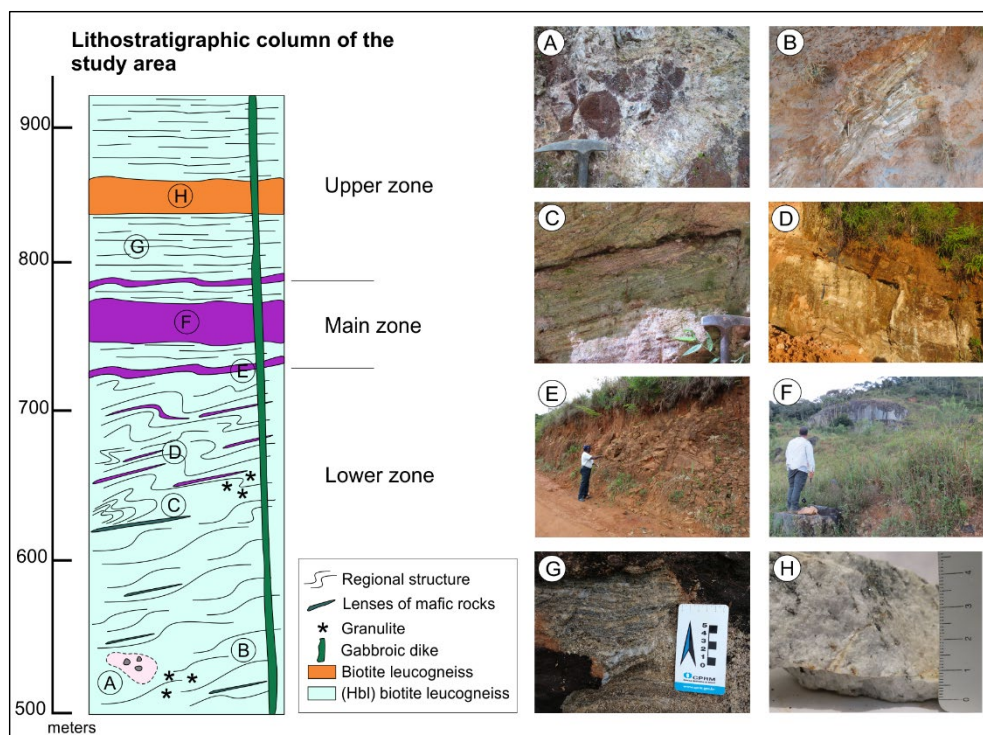


Figure 4: Schematic representation of the lithostratigraphic zoning in the Aracitaba region. At the base of the low zone: **(A)** mafic enclaves in the quartz-feldspathic rock body; **(B)** Parasitic folds in weathered outcrops of (hbl) biotite gneiss; and **(C)** mylonitic foliation with intrafolial folds. Top of the low zone: **(D)** thin amphibolite lenses in sharp contact with biotite gneiss. In the main zone: **(E)** four-meter layer of garnet metagabbro, marking an increase in the thickness of the layers; **(F)** mine disabled where the largest body of garnet metagabbro outcrops. Upper zone: **(G)** the return of (hbl) biotite gneiss with compositional banding that transition to the lithotype; **(H)** biotite leucogneiss.

this prospective campaign for the investigation of Fe-Ti-V oxides. In general, it occurs with little variable mineralogical composition, with a massive structure and gray to greenish-gray coloration.

The lithotype has a positive, but low susceptibility, with an average of 1.36×10^{-5} (SI). It often outcrops as in situ blocks, or as outcrops in road cuts. When in sharp contact with the biotite gneiss, it shows, several times, a rapid increase in the topographic gradient and significant relief breaks in the terrane. The upper zone (UZ) is marked by the reappearance of (hornblende) biotite gneiss, which presents a marked compositional banding, formed by alternating mafic (biotite and hornblende) and felsic (quartz and feldspar) bands (Figure 4G). The banded biotite gneiss is overlaid by a layer of biotite leucogneiss (Figure 4H), which transitions back to (hornblende) biotite gneiss when in proximity to the top of UZ.

Along the zones, it is possible to observe the regional structure trend. In the central portion of the area, it can be seen structures with a predominant

NW-SE trend and dip ranging between 10 and 30 degrees to the NW direction, while in the northern portion, the foliation inflects to the NE-SW direction, at low to medium angles to the SE direction. It was noted that the NE-SW direction is associated with more recent structures, which cut through deformed rocks, such as low-angle shear zones, faults, and intrusions of gabbroic dykes. These lithotypes are not differentiated in the geological map, as they do not outcrop on the surface, probably due to the low diving angle of the rocks in the region. They are often found in cuts on the side of the road or as blocks in situ.

Petrography

Based on the mineralogical composition (Table 2) and textural characteristics, five main lithotypes were characterized: garnet metagabbro (Figure 5), amphibolite, granulite, gabbro (Figure 6) and (hornblende) biotite gneiss (Figure 7). The garnet metagabbro lithotype has an essential mineralogy

consisting of pyroxene, plagioclase, garnet, ilmenite, magnetite, and apatite (Figure 5A). The pyroxene is partially or replaced by hornblende, actinolite, and, subordinately, by chlorite (Figure 5B). The plagioclase is arranged as subhedral, tabular crystals with irregular edges, showing different degrees of alteration, and may even be partially recrystallized (Figure 5C). It was also observed tiny tabular and euhedral plagioclase crystals embedded in pyroxene crystals.

The metagabbro garnet presents heterogeneous deformation characterized by areas almost completely preserved, with slightly deformed regions with incipient foliation (Figure 5D), and others intensely deformed, where they show greater plagioclase recrystallization and stretching of the crystals. In general, this rock type is localized in areas with deformation, or with very incipient deformation. Exposure ophitic, subophytic, and even porphyritic relict textures with preserved plagioclase phenocrysts in the middle of the plot predominate in this unit (Figure 5E).

The main oxide found in this rock is ilmenite, which varies from 8 to 12%, while magnetite is disseminated in the section with up to 3%. Ilmenite is found alongside mafic minerals exhibiting skeletal shapes. In some points, it occurs surrounded by biotite and chlorite (Figure 5F); in others, in association with hornblende and titanite, which are arranged as oriented clusters or trails; and it can still be found in symplectic intergrowth with garnet. The pyrite and apatite are accessory phases, being sparsely distributed. The pyrite occurs punctually. The apatite shows hexagonal shapes in the basal section. The biotite forms lamellar and ripiform crystals, in disagreement with the orientation of the matrix grains, suggesting late formation. The sericite and calcite occur because of a secondary alteration of the plagioclase.

The granulite lithotype has a massive structure and a gray-green color (Figure 6A). It consists mainly of crystals of augite, hypersten, plagioclase, quartz, garnet, magnetite, ilmenite, and apatite. The rock has a granoblastic, coronitic, and sometimes polygonal structure, where crystals exhibit regular polygonal shapes forming triple points (Figure 6B). The occurrence of hornblende, actinolite, and cummingtonite is common, replacing the edges and interior of pyroxenes and in

the overgrowth of the biotite near the edges of the amphibole. The garnet forms crowns around the pyroxene (Figure 6C) and amphibole. Subordinated, it can also be observed involving the opaque minerals and exhibiting symplectic intergrowth structures with ilmenite. The magnetite occurs at 5 – 7%, while the ilmenite does not exceed 4%. The apatite is disseminated in the rock in the form of small sub-rounded grains, included in the plagioclase. Secondary minerals such as muscovite and calcite correspond to the product of secondary alteration of the plagioclase, appearing in its interior, edges, and cleavages.

The amphibolite rock has a grayish-black color, showing a foliated or laminated structure, and fine to medium grain (Figure 6D). Its mineralogy consists of hornblende, plagioclase, quartz, apatite, oxides, and sulfides, with or without garnet. It has a nematoblastic texture (Figure 6E), where hornblende and plagioclase crystals are recrystallized and parallelized according to the deformation direction.

The oxides, ilmenite and magnetite, titanite, apatite, and sulfides represent accessory phases and are found widespread in the rock. The rock has a mylonitic texture when associated with shear zones. The gabbro outcrops as blocks in situ, characterized as a dyke with a trend varying between NE/010 and NE/030. It represents the only igneous lithotype in the area. It has a dark gray color, massive structure, and fine to medium particle size (Figure 6G). Its mineralogy is essentially formed by augite, plagioclase, magnetite, and to a lesser extent, ilmenite, and quartz. The rock exhibits a porphyritic texture, where euhedral to subhedral phenocrysts of augite and plagioclase (Figure 6H) can be observed, surrounded by a fine matrix formed predominantly by andesine. Augite phenocrysts form glomeroporphyritic clusters in the matrix. The augite occurs in euhedral to subhedral form, often exhibiting magnetite inclusions (Figure 6I). The oxides occur in a disseminated form throughout the entire lamina and present a fine granulation, not exceeding 1mm. This growth may indicate a crystallization stage after the phenocryst formation phase, together with the plagioclase that forms the matrix.

The (hornblende) biotite gneiss covers most of the area, occurring with varied structures depending on the degree of deformation involved throughout the region.

Table 2: Average of the semi quantitative modal analysis of the lithotypes characterized in the area.

Lithotype Minerals (%)	Garnet Metagabbro	Amphibolite	Granulite	Gabbro	(Hbl)
					Biotite gneiss
Pyroxene	5 – 7	-	36 – 40	35	-
Plagioclase	35 – 38	12 – 16	35 – 37	44	30 – 35
Magnetite	2 – 3	2 – 3	5 – 7	8	-
Ilmenite	8 – 12	2 – 4	2 – 4	3	-
Pyrite	< 1	< 1	-	-	<1
Hornblende	32 – 36	65 – 70	2 – 3	-	1 – 3
Actinolite	3 – 7	-	2 – 3	-	-
Garnet	4 – 6	0 – 2	3 – 7	-	-
Chlorite	1 – 2	-	-	5	-
Biotite	2 – 4	3 – 5	3 – 4	-	2 – 8
Quartz	7 – 9	10 – 12	5 – 7	3	10 – 15
Microcline	-	-	-	-	22 – 25
Ortoclase	-	-	-	-	28 – 30
Apatite	2 – 5	<1	< 1	2	< 1
Titanite	2 – 4	2 – 3	-	-	2 – 3
Muscovite	-	-	< 1	-	< 1
Calcite	-	-	< 1	-	< 1

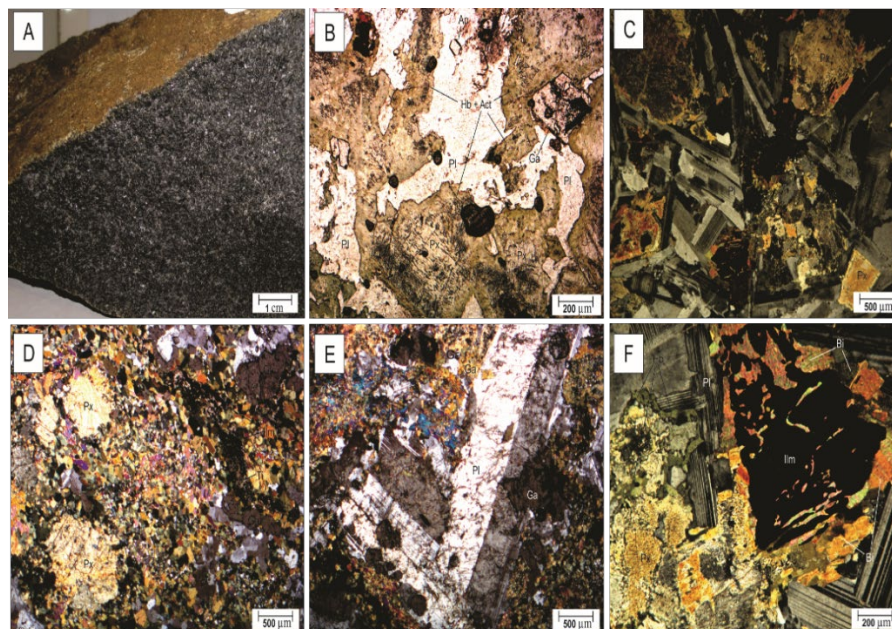


Figure 5: Mineralogical composition and textural characteristics of the garnet metagabbro. **(A)** Massive and homogeneous structure. **(B)** Photomicrographs of the lithotype showing pyroxene relict with edges replaced by a mixture of amphibole (hornblende + actinolite). **(C)** Tabular plagioclase crystals showing slightly recrystallized edges. **(D)** Matrix of finely recrystallized amphibole and ilmenite trail with titanite oriented according to incipient foliation. **(E)** Phenocrystal relict of plagioclase. **(F)** Skeletal ilmenite in contact with biotite and chlorite.

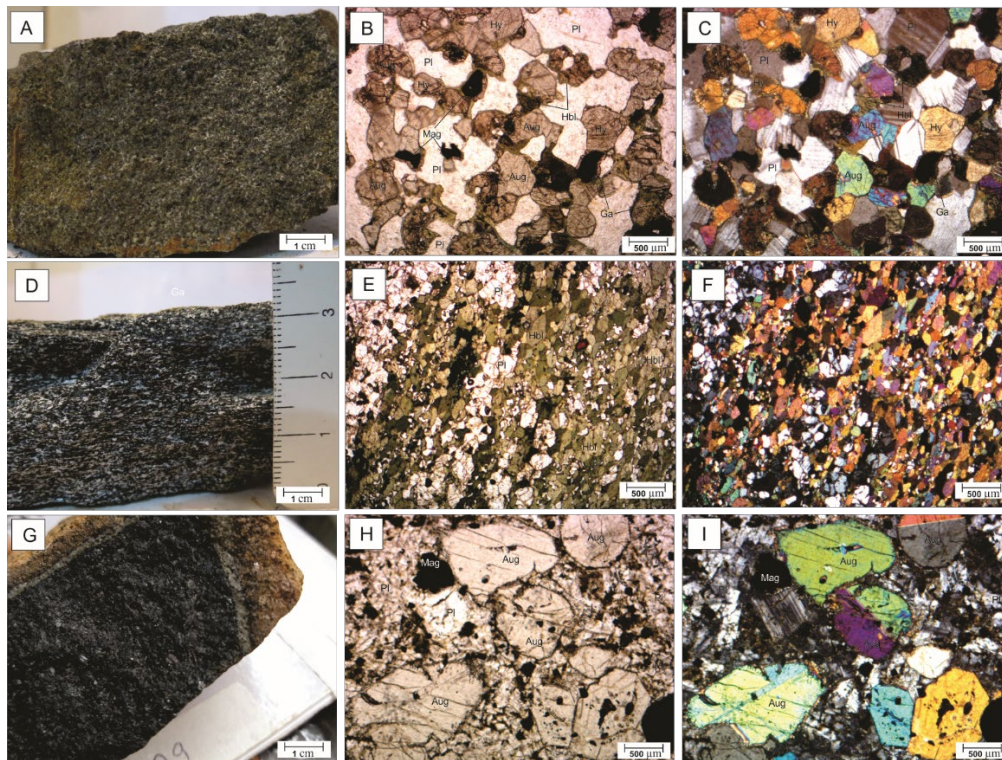


Figure 6: Sample of: **(A)** granulate showing massive structure; **(B)** photomicrographs of the lithotype showing garnet (Ga) coronitic involving crystals of augite (Aug) and magnetite (Mag); **(C)** photomicrograph of the lithotype showing granoblastic texture formed by hornblende, plagioclase and quartz; **(D)** amphibolite garnet with massive structure; **(E)** photomicrographs showing fine-grained nematoblastic texture; **(F)** hornblende crystals paralleled according to the preferential direction of foliation; **(G)** a specimen of gabbro showing massive structure; **(H)** photomicrographs showing porphyritic texture with subhedral crystals in the matrix; **(I)** augite crystals with inclusions of magnetite and ilmenite.

The essential mineralogy of the lithotype (hornblende) biotite gneiss consists of biotite, quartz, plagioclase, microcline, and orthoclase. Opaque minerals and titanite are accessories in the rock. The titanite occurs surrounding the opaque minerals and can occur in the form of agglomerates. The hornblende may occur in small quantities or be absent from the lithotype. The rock has a granolepidoblastic texture given by the alignment of biotite crystals in it (Figure 7A). In some points, the biotite leucogneiss variety occurs in the region. In the rock, a predominance of microcline, orthoclase, plagioclase, and quartz is observed, giving the rock an inequigranular granoblastic texture, while micas, biotite, and muscovite occur in a secondary form (Figure 7B). The titanite and opaque minerals are accessory phases, and garnets may be present in the rock.

Magnetometry Method

Magnetic anomalies evidence the structural framework and the presence of mafic lithotypes in the area. The magnitude of the anomalous magnetic field varies a

lot (Figure 8A). Observing the high values for the amplitude of the analytic signal (Figure 8B), which facilitate the spatial location of these anomalous magnetic sources, it can be determined the magnetic highs values in the order of 118 nT are related to the metagabbroic rocks in the region. The minimum values for magnetic intensity in the order of -67 nT are related to the exposed gneiss lithotypes, which are generally quite weathered.

Magnetic Domains

To classify these magnetic domains, it was used the distribution of the amplitude values of the analytic signal (Figure 8B), where each one of the three classified domains (ASA1, ASA2 and ASA3) corresponds to a range of values observed in this map. This map comprises anomalies with values ranging from 0.0005 nT/m to 1.3366 nT/m. The domains classified have a range correspondence in the amplitude signal: ASA1 is associated with the values > 0.059 nT/m; ASA2 with the values between 0.015 and 0.059 nT/m; and ASA3 with the values < 0.015 nT/m.

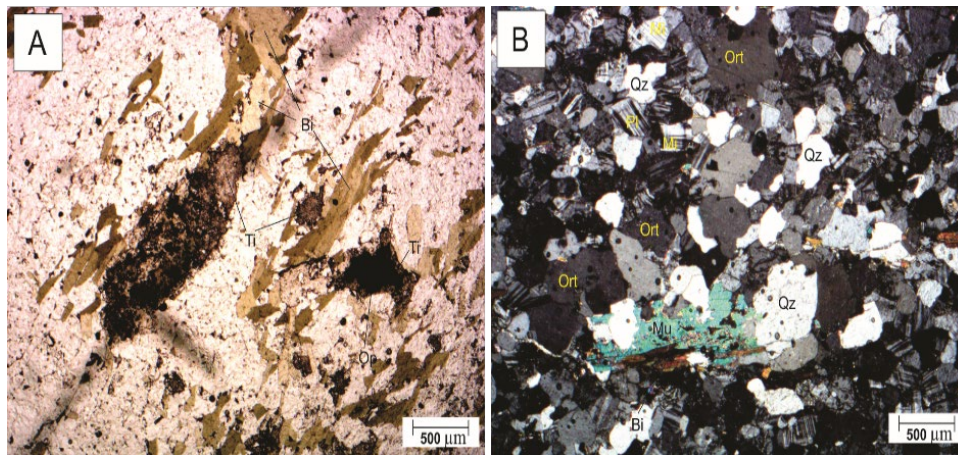


Figure 7: Photomicrograph of (hbl) biotite gneiss showing (A) granolepidoblastic texture given by the alignment of the biotite (Bi) and titanite (Ti); (B) Inequigranular granoblastic texture showing microcline (Mi), orthoclase (Ort), muscovite (Mu) and biotite.

In the ASA1 domain, the regions with high magnetic amplitude are highlighted with structures oriented in the general NE-SW direction and subordinated in the E-W and WNW directions. It features linear shapes and also some magnetic bodies which are isolated structures without lateral continuity, but with high magnetic amplitude.

The ASA2 domain consists of anomalies with relative intermediate magnetic magnitudes, which are narrow and present an elongated shape. Despite presenting discontinuous features laterally, continuity trends are observed in the WSW-ENE and NW-SE directions. The ASA3 domain is characterized by low magnetic regions, which follow in the direction of domain 2.

Magnetic Lineaments

Vertical derivatives act as high pass filters that enhance the high frequency/short wavelength content of the data and suppress low frequency/long wavelength signal. The first vertical derivative ($n=1$) enhances rapid changes in the magnetic field at the edges of the anomalies, and therefore it is useful for delimiting the extents of causative bodies. Thus, using shading and lighting techniques, it is possible to highlight linear features in this map that may be correlated to geological contacts with magnetic contrast in the subsurface. In the vertical derivative (DZ) map, the interpreted lineaments (Figure 9) have values between -0.823 nT/m and 0.792 nT/m. In the zones of greater magnetic amplitude, it was possible to highlight the edges of the magnetic bodies and lineaments present in the region and their distribution in the area, emphasizing the direction of structures with medium to low values (Figure 9A).

In the Tilt derivative map (Figure 9C), the amplitudes were equalized to highlight the center of the magnetic bodies and their continuity. The Figure 9D shows the magnetic lineaments derived from Figure 9C. The linear magnetic features identified in both images (Figure 9B and 9D) were classified into four (4) classes according to the preferred direction, lateral continuity, and magnetic amplitude of the anomaly (Table 3). The L1 lineaments coinciding with the bodies highlighted by the analytic signal occur in the NE-SW direction.

The L2 lineaments represent continuous curved segments with a high magnetic response, with different directions around the E-W. The L3 lineaments show secondary magnetic features, whose magnitude of the anomaly present values from intermediate to low amplitude, while the L4 lineaments are characterized by an intermediate to low magnetic amplitude in the NE-SW direction. From the interpreted lineaments, an overlap of the defined classes was identified. The correlation between the structures in the different maps are shown in Table 3, within which three structural patterns were obtained.

Radiometry Method

The radiometric maps, the basis for geochemical interpretations of the distribution of natural radioelements in the region, were generated from the interpolation of the K, equivalent uranium (eU) and equivalent thorium (eTh) channels, duly corrected, using the minimum curvature method (Briggs, 1974), and are illustrated in Figure 10. The corrections of gamma spectrometric data obtained from both ground and airborne surveys must follow the recommendations specified in the technical reports developed by the International Atomic Energy Agency (IAEA, 1991, 2003).

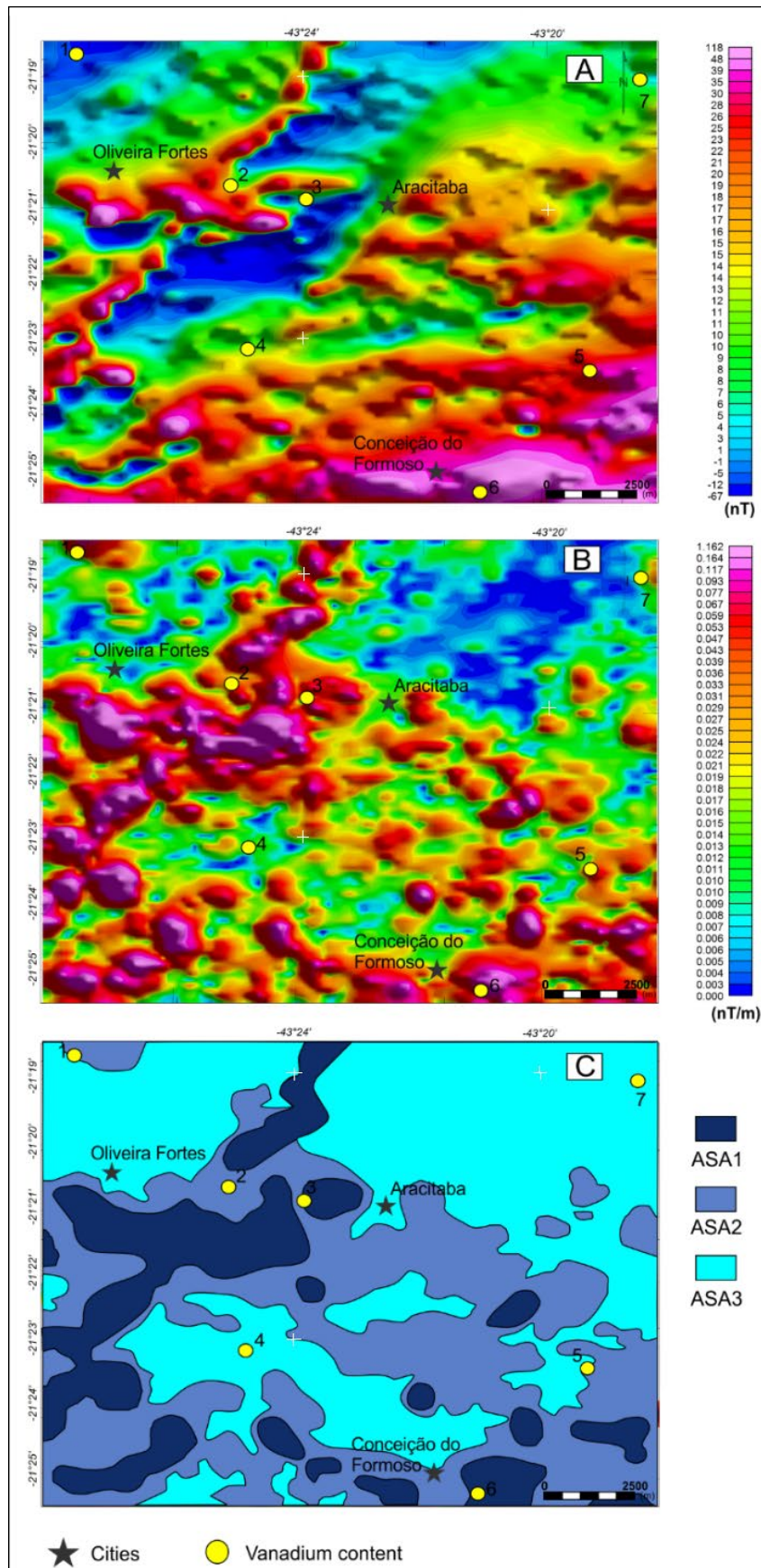


Figure 8: Magnetic maps: (A) Anomalous magnetic field (AMF); (B) Analytic signal amplitude (ASA); (C) Magnetic domains.

Table 3: Correlation between magnetic lineaments and structural patterns.

DZ	TDR	Description	Structural pattern and geological description	
L1	L1	Extensive and continuous lineaments	1	Dykes (Gabbroic rocks) NE-SW
L2	L2	Curvilinear and continuous segments with variable direction - Mainly in the E-W direction	2	Folds and regional foliation associated with metagabbros and amphibolites E-W / NW-SE / ENE-WSW / WNW-ESE
L3	L3	Secondary lineaments		
L4	L4	Continuous lineament	3	Mylonitic foliation and Shear zones NE-SW / ENE-WSW

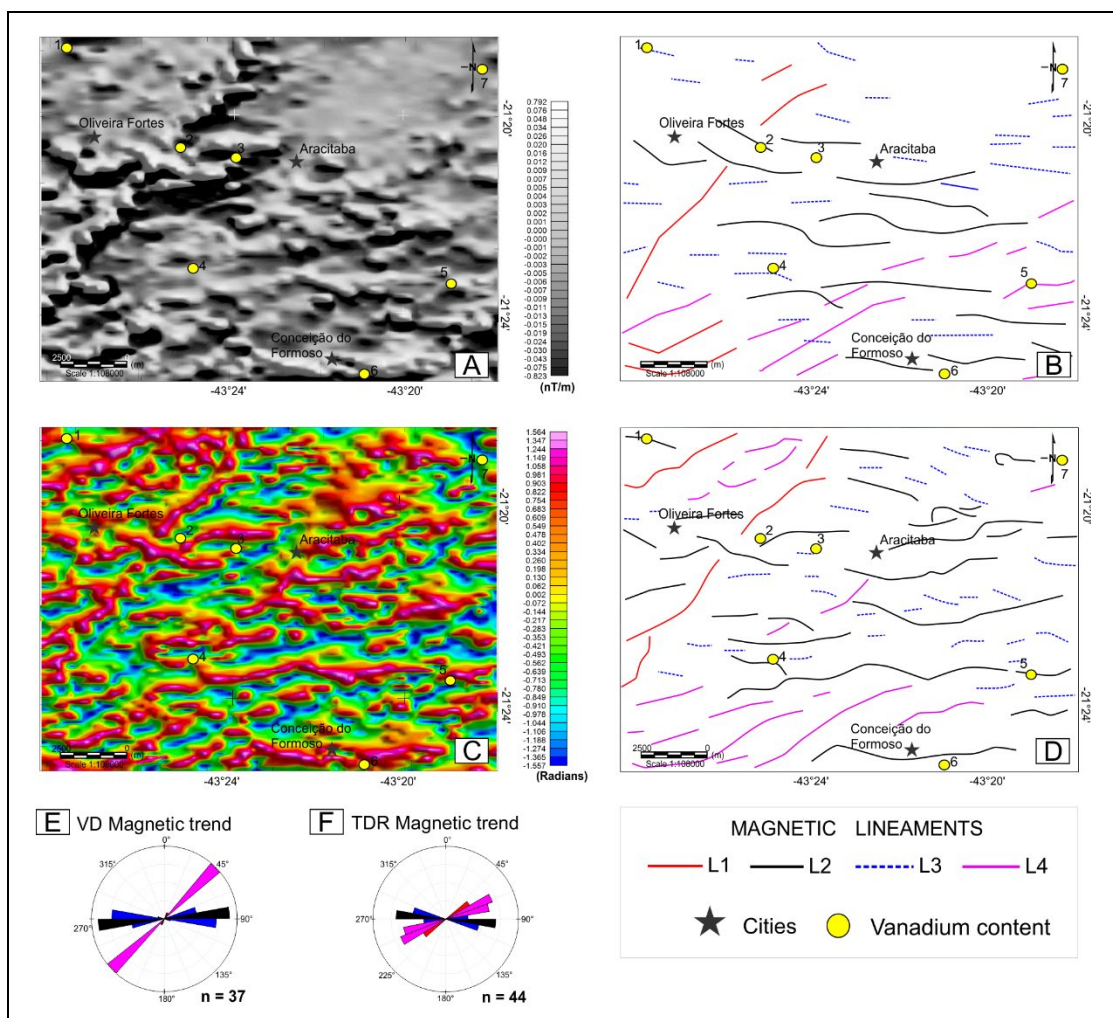


Figure 9: Images and magnetic lineaments: (A) Vertical derivative (DZ); (B) Lineaments obtained from the DZ map; (C) Tilt derivative (TDR) and (D) Lineaments obtained from the TDR map; Rosette diagram showing the NE-SW, NW-SE and E-W trends obtained through the magnetic lineaments of the (E) DZ map and (F) TDR map.

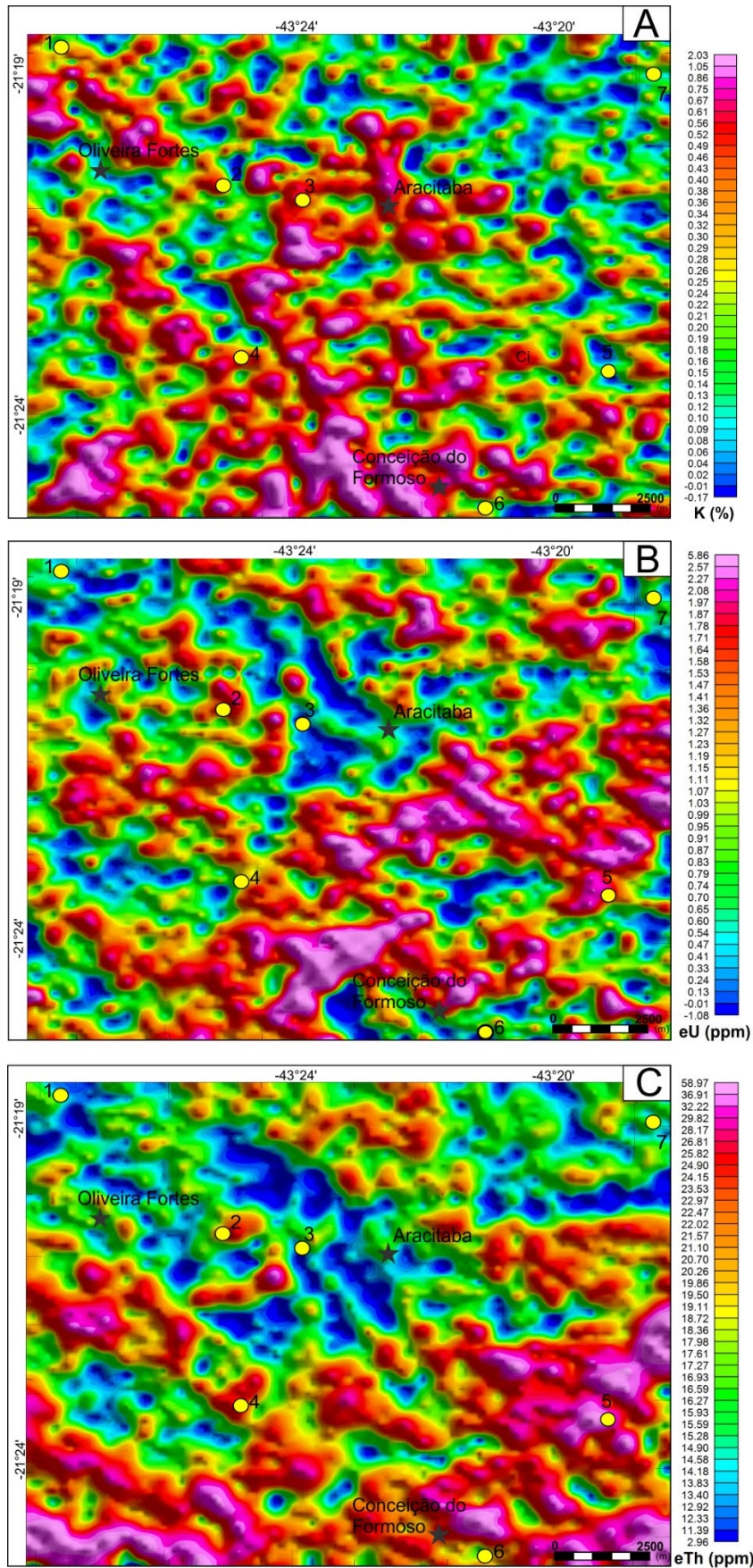


Figure 10: Concentration map of the (A) K (%); (B) eU (ppm); and (C) eTh (ppm) channels. The yellow dots in the figure indicate vanadium occurrence and the stars refer to the main cities of the region.

For this, the “dead time” correction, the calculation of the effective flight height, Compton scattering, background radiation (BKG) and altimetric correction are considered.

The highest levels of potassium ([Figure 10A](#)) are found in the northern portion, exhibiting a persistent NW-SE trend, while the concentrations of thorium ([Figure 10B](#)) and uranium ([Figure 10C](#)) are found mainly in the southern part, showing a directional component to the NE. In the potassium map, it is possible to observe concentrations up to 2.03%, where the highest concentrations are found mainly in the central portion of the area and the little less expressive ones in the NW region. The eTh concentration varies between 2.96 and 58.97 ppm, and the eU values reach 5.86 ppm in the region.

Despite the difference in concentration of these elements in the region, they tend to occur together in the area. In the thorium concentration map ([Figure 10B](#)), it is possible to observe that, in the northern area, the high to median eTh contents constitute a trend in the NW-SE direction, while in the southern one, this direction changes to NE-SW. In the uranium concentration map ([Figure 10C](#)), this trend persists, albeit discreetly.

Ternary image and interpreted lithogeophysical map

A ternary map ([Figure 11A](#)) captures the relative and absolute levels of radiation of the principal natural radioelements. It is generated using the RGB standard configuration, associating the colors red, green, and blue to potassium (in %), and the counts of eTh and eU (in ppm), respectively. Eight lithogeophysical domains were interpreted, based on the intensity of each radioelement in the area ([Table 4](#)). The lithogeophysical domains were classified from A to H ([Figure 10B](#)) and refer to a qualitative comparison between geological and radiometric characteristics of the study area ([Table 5](#)). The radiometric maps indicated a predominant overlay of the region by gneiss rocks, and only a preferential sector correlated with mafic lithotypes (unit H).

From the geological mapping work, and based on the interpreted geophysical maps, a new geological map was elaborated, integrating the compiled geological data and new data acquired from the fieldwork and the interpretation of the geophysical maps ([Figure 12](#)). The discriminated lithogeophysical units were correlated to the geological map of the area, corresponding, almost

entirely, to the gneiss rocks of the region. The H unit was correlated to basic characteristic rocks, mainly due to the low quantity of associated radioelements, and the direct relationship with the ASA3 magnetic domain, characterized by high magnetic amplitude in the magnetic maps.

The 720-ppm vanadium anomaly, found in a low magnetic amplitude domain, is coincident with the lithogeophysical unit G, which is associated with a drainage zone. This configuration suggests that the lithotype used for sampling was in the vicinity of the drainage. It was transported a short distance since there are outcrops of the garnet metagabbro in the vicinity.

DISCUSSION

Data integration and magnetic signature

Regarding the magnetic data, the domain map elaborated based on the ASA is directly correlated to the metagabbros, amphibolites, granulites and to the mapped structures, such as foliation, shear zones and dykes. However, most of them have no surface representation. According to [Pinto \(1995\)](#), the distribution of metagabbros on the surface is irregular, presenting different thicknesses, characterized by lenses distributed throughout the gneiss sequence associated with São Bento dos Torres Suite. [Hiraga et al. \(2017\)](#), on the other hand, characterizes the same metabasic rocks as sills (Oliveira Fortes unit) within the sequence of rocks of the Conceição do Formoso Group, formed by biotite leucogneisses and hornblende biotite gneisses. Therefore, the magnetic data measured generate a low correlation with the geological maps covering the investigated area.

The garnet metagabbro and granulite lithotypes generally have a high magnetic response, which matches the ASA1 domain, differing from the amphibolite found in the ASA2 domains. This fact is due to the different metamorphic conditions and distinct paragenesis found for these lithotypes, which implies different magnetic responses. According to [Clark et al. \(1992\)](#), gabbros metamorphosed into greenschist and amphibolite facies have low susceptibilities and are generally weakly magnetic because of superimposed metamorphism. This is because high-grade metamorphism favors the occurrence of mineralogical substitutions that directly influence the decrease in magnetic susceptibility. This fact is corroborated by the different paragenesis found

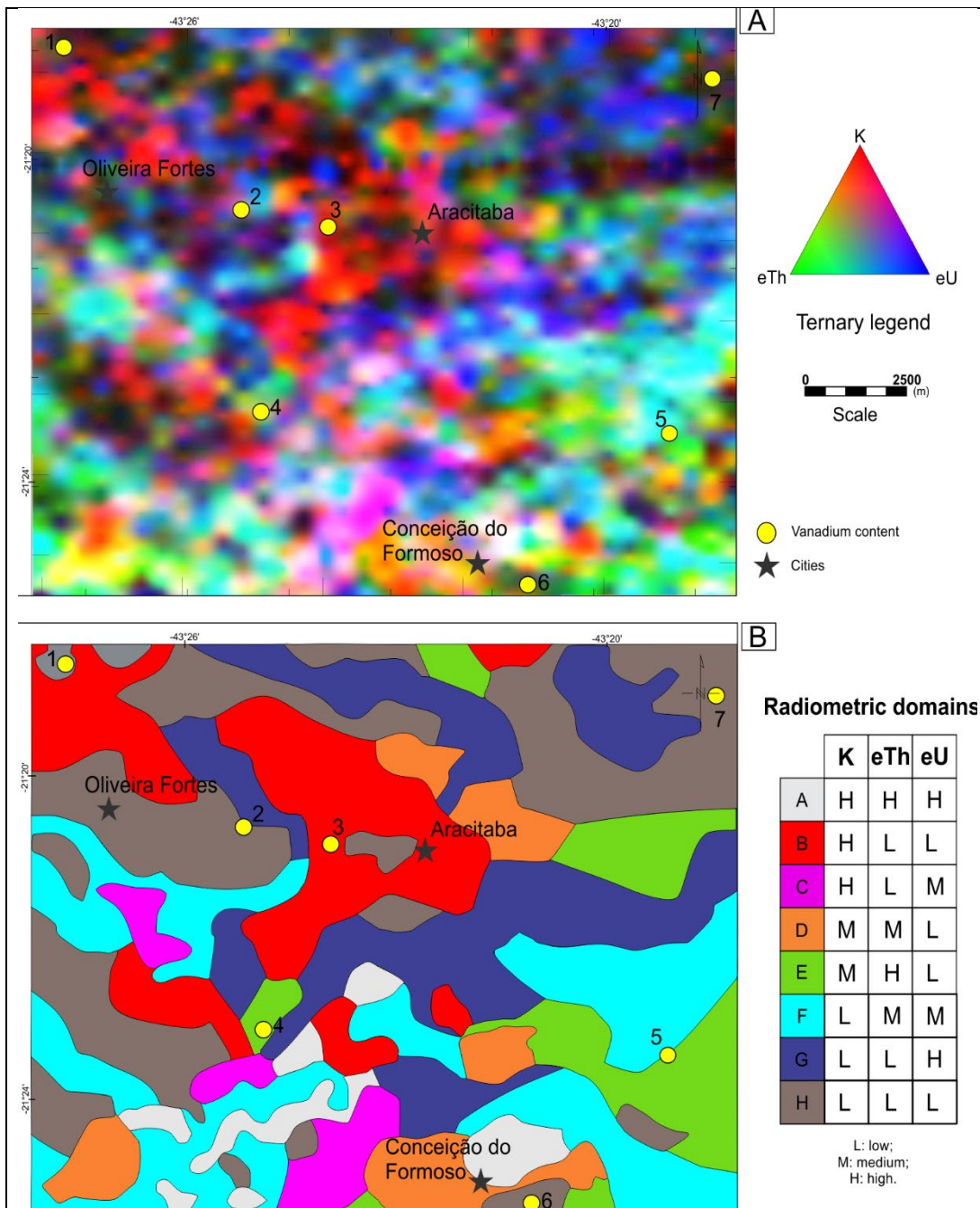


Figure 11: Concentration map of the (A) K (%); (B) eU (ppm); and (C) eTh (ppm) channels. The yellow dots in the figure indicate vanadium occurrence and the stars refer to the main cities of the region.

Table 4: Intensity of radioelements used in the interpretation of radiometric maps.

Radioelements	Low	Medium	High
K (%)	< 0.25	0.25 – 0.60	> 0.60
Th (ppm)	< 19.00	19.00 – 28.00	> 28.00
U (ppm)	< 1.10	1.10 – 1.80	> 1.80

Table 5: Description of radiometric lithogeophysical domains interpreted in the study area. Responses for K, eTh, eU are L – Low; M – Medium; H – High.

Domain	Responses			Lithological correlation	Description
	K	eTh	eU		
A	H	H	H	(Hbl) Biotite gneisses	It corresponds to small areas located in the central and southern regions of the map.
B	H	L	L	Altered (hbl) biotite gneisses	Altered gneiss from low topographic areas in the South, and high areas in the North, which covers the metagabbros (Trend NW-SE).
C	H	L	M	Colluvium	Drainage region, characterized by superficial mobilization. It tends to expose weathered gneiss outcrops.
D	M	M	L	Altered (hbl) biotite gneisses	It tends to expose weathered gneiss outcrops on median slope.
E	H	M	L	Colluvium	Drainage area.
F	L	M	H	Altered (hbl) biotite gneisses and colluvium	There are high areas with outcrop (Hbl). Biotite gneisses supported by intercalations of metabasites in the middle of the package (western). The decrease in topography indicates a zone of secondary accumulation in the eastern portion.
G	L	L	M	Altered biotite gneisses	Middle slope with U mobilized from the highest units. In the western and southern portions of the map, it coincides with the ASA3 domain.
H	L	L	L	Mafic rocks (Metagabbros, amphibolites and granulites)	Characterized by radioelements depletion. In the North and South, the unit is related to topographically high areas, where the mountain range is supported by metagabbros. In the extreme Southeast of the map, it is related to topographic lows. It coincides with the ASA1 magnetic domain, being probably associated with unmapped metabasites.

for the metagabbro. These materials reveal conditions of regional metamorphism in medium to high amphibolite facies, and locally, in granulite facies, in agreement with [Hiraga et al. \(2017\)](#).

The moderate magnitude anomalies of the ASA2 domain show a correlation mainly with amphibolite, found in the thin intercalations amidst the (hornblende) biotite gneiss. This rock has a low content of magnetite (2-3%) and ilmenite (3-5%) according to petrographic analyses. [Clark \(1999\)](#) relates the significant loss of magnetic properties of metabasic rocks to the increase of the temperature caused by metamorphism, allowing the occurrence of phases rich in iron and titanium in

magnetite and retrometamorphic processes along shear zones, which can provide local magnetic variations. The ASA3 domain, on the other hand, was correlated with gneiss lithotypes, characterized by a low content of magnetic mineralogy. They are usually found quite altered, in intensely denuded regions.

The larger NE-SW magnetic lineaments (Pattern 1) were correlated to late igneous intrusions, such as the gabbroic dyke found in fieldwork (e.g., CM-08) in the extreme west of the area. Other guidelines occur in the NW-SE and NNE-SSW directions, many of which were used for the installation of local drainages. The presence of granitic rocks, associated with these lineaments,

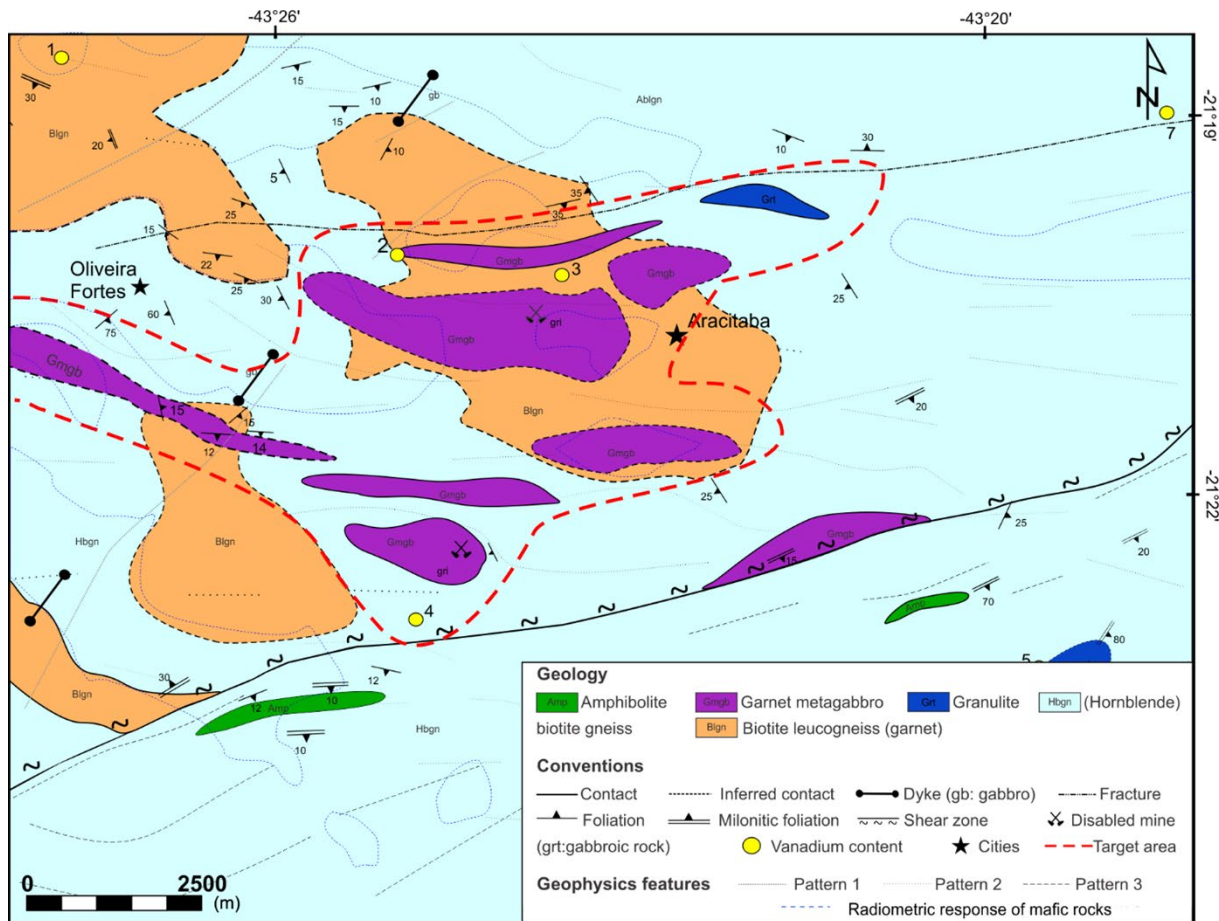


Figure 12: Geological map of the study area with geophysical integration showing the selected target area.

presupposes that some of them correspond to geological faults and evidence of partial melting of biotite gneiss, with assimilation of enclaves of mafic composition.

The structures with higher density in the area are associated with Pattern 2. The variations in the directions (EW / NW-SE / ENE-WSW / WNW-ESSE) discriminated in the images were correlated to the folds in the region, resulting from the tectonic evolution of this portion of the Ribeira Range. The low-angulation shear zones, indicated by Hiraga et al. (2017), are evidenced, in general, by the mylonitic features in amphibolite garnet and (hornblende) biotite gneiss. The garnet metagabbro and garnet amphibolite lithotypes are found in the field as intercalated bodies of different thicknesses amidst the gneiss rocks, in general, presenting foliations with a W-E and NW-SE direction and with a low-angle dip. According to Heilbron et al. (2000, 2004) and Almeida (2000), in a regional context, these structures would be associated with late deformation phases, which redouble the main foliation, and can be recognized in the field opening to tight folds.

NW-verged low-angle shear zones (Brandalise et al., 1992; Hiraga et al., 2017) are correlated to the linear

structures of Pattern 3 and are characterized by NE-SW trend lineaments in magnetic images. Heilbron et al. (2000, 2004) attribute structures like these to ductile shear zones installed during the main folding phase, which become push zones, being marked by mylonitic rocks and a strong stretch lineation, with the amphibolites found in the region.

Data integration and radiometric signature

With regard to radiometric data, interpretations turned to understanding the distribution of metagabbros in the region, since the vanadium anomaly is strongly associated with the occurrence of lithotypes of gabbroic composition, as shown by studies carried out in different deposits of the world (Abu El-Ela, 1996; Kärkkäinen and Bornhorst, 2003; Sarapaa et al., 2005; Hou et al., 2012; Zhou et al., 2013), and also in the context of the Ribeira Belt (Pereira et al., 2016; Vaz et al., 2017), corresponding to the metallotect Fe-Ti oxides in the studied area.

The lithogeophysical units indicated in the ternary image reflect the distribution pattern of the

radioelements K-U-Th on the surface ([Wilford et al., 1977](#)). In general, this content is quite variable, and this reflects the lithological and structural complexity of the study area, which belongs to a highly deformed sector of the Ribeira Belt. In this way, the geological maps that cover the region are very different products and are not easily related. The São Bento dos Torres Suite, proposed by [Brandalise and Viana \(1993\)](#), encompasses metagabbros, biotite gneisses and amphibolites in a single unit. [Hiraga et al. \(2017\)](#) define two units to represent the gneissic and metabasic lithotypes, contributing to a representation that is more compatible with the local geology. However, the correlation of geology with radiometric units revealed wide divergences.

Significant changes in geology have been proposed for the area, considering the radiometric response of the gneiss bodies in contrast to the gabbroic ones. The central region of the map, where the metagabbros are concentrated, is covered by the lithotypes (hornblende) biotite gneiss and biotite leucogneisse, and despite the varying degrees of alteration in which they are found, the radiometric response is compatible with the interpreted lithogeophysical domains, since they are characterized by the rhyolitic dacitic composition according to [Hiraga et al. \(2017\)](#). This stacking is clear in the lithostratigraphic zoning proposed for the region.

The biotite leucogneisse variety has a high content of K-feldspar, microcline and orthoclase. This content is compatible with the gamma ray spectrometric signature of domains A, B and C, characterized mainly by high potassium content, which made possible a distinction of the hornblende biotite gneiss and the biotite leucogneisse lithotype. This fact is supported by [Dickson and Scott \(1997\)](#), who state that rocks tend to have an increase in the percentage of K-Th-U according to the silica content, where felsic rocks have higher values, while intermediate rocks, mafics or ultramafics are characteristically more impoverished in these radioelements.

As this is an area heavily affected by weathering processes, a depletion of K is observed, mainly in the lowland areas belonging to unit G and part of unit F, where altered gneisses and residual soils predominate. This signature points out to a possible process of releasing K from the K-feldspar and a biotite structure for the formation of clay minerals ([Ulbrich et al., 2009](#)). On the other hand, Th and U occur in minerals resistant to weathering and with low dissolution under the influence of aqueous solutions, with greater

possibility of selective concentration by mechanical processes ([Dickson and Scott, 1997](#); [Wilford et al., 1997](#)). Thus, the radiometric response in the drainage areas and topographically lower, indicated by high concentrations of Th, is compatible with Th values directly associated with healthy rock, or with secondary accumulations in the soil.

Unlike the gamma-ray spectrometric signature of the gneisses, the metagabbros are indicated by the absence of a response, which reflects the impoverishment in K-Th-U. This contrasting signature, together with the anomalies identified in the ASA1 magnetic domain, highlighted important structures and outcrops of metagabbros, also found in areas not previously identified, playing a relevant role in this phase of the geological exploration, which aims to select target areas.

CONCLUSIONS

The aerogeophysics methods was applied to discriminate gabbroic bodies, considered potential areas for vanadiferous mineralization, by their Fe-Ti oxide content, based on the magnetic and gamma ray spectrometric signature of the study area. The differentiation between mafic and felsic lithotypes and the characterization of the structures are based on magnetic anomalies highlighted in the geological environment. The aeromagnetic responses for the garnet metagabbro and gabbro are similar; both give rise to strong magnetic anomalies but differ in the form of occurrence.

The metagabbro occurs in the form of elongated bodies (NW-SE) and has a higher content of ilmenite compared to the magnetite, presenting a positive magnetic response, which differs from the gneiss lithotypes due to low or absent magnetic responses. The tectonic framework is reflected in the main structural lineaments traced in the NW-SE, NE-SW, E-W directions. The radiometric signature of the metagabbro is based on the depletion of the radioelements K-eU-eTh on the surface, showing a correlation with unit H. The abundance of K, U and Th is low when compared to acid and intermediate rocks (e.g., [Boyle, 1982](#)). As for the radioelements during the weathering and in soil/regolith see, for example, [Dickson and Scott \(1997\)](#), [Wilford et al. \(1997\)](#) and [Ulbrich et al. \(2009\)](#). Uranium and thorium tend to concentrate in soils derived from mafic and ultramafic rocks (see [Figures 4 and 5](#) in [Dickson and Scott, 1997](#)).

The integration map of the units presents the geology of the area different from the proposals by [Brandalise and Viana \(1993\)](#) and [Hiraga et al. \(2017\)](#), as it focuses on the distribution of the garnet metagabbro lithotype and its relationship with host rocks, based on the magnetic and radiometric responses to guide mineral prospecting. Despite the differences observed, the map collaborated to identify areas favorable to the occurrence of metagabbro, mainly due to the presence of few rocky outcrops and regions with difficult access.

The lithostratigraphic zoning was proposed to characterize the rocks in the region and helped to understand the gaps left by ambiguities in the geophysical maps due to the geological complexity. The division into zones showed the positioning of the garnet metagabbro in the main zone, embedded in the gneiss rocks. It is still possible to identify a progressive decrease in the influence of regional deformations towards the main zone, possibly because the metagabbroic rocks kept the primary structures preserved.

The different geophysical maps allowed the differentiation of lithotypes, characterization of domains and lineaments based on contrasting magnetic properties, and the geochemical distribution of the radioelements in the geological environment. Magnetic maps, anomalous magnetic field (AMF) and its products, vertical derivative (DZ), Tilt derivative (TDR) and amplitude of the analytic signal (ASA) were useful in the characterization of anomalies, domains and magnetic lineaments. From these maps, it was possible to delimit bodies, correlated to the basic and metabasic lithotypes, and trace lineaments in the NW-SE, NE-SW, EW directions, coinciding with the structural patterns found in the literature and during the geological mapping work in the region.

Most of the selected target areas, including the 720-ppm vanadium anomaly, coincide with the outcrops mapped as metagabbro, making these locations important potential areas of Fe-Ti-V oxide concentration as they coincide with NW-SE trending magnetic anomalies, pointing out to a lithologic-structural control. Finally, the use of magnetic and radiometric data as an aid tool in mineral exploration campaigns proved to be an important research front aimed at prospecting Fe-Ti-V oxides, where the integration of geophysical and geological data was essential in the preparation of the integrated geological map of the study area and indication of the garnet metagabbro, target of this prospective campaign.

ACKNOWLEDGMENTS

The authors would like to thank Dr. Giuliano Marotta, deputy editor of the BrJG, for handling our manuscript as editor, and the two anonymous reviewers (2nd review) for their helpful comments that considerably improved our work. The authors are grateful to FAPERJ for the scholarship and to the Postgraduate Program in Geosciences (PPGG) of the Geology Department of the Rio de Janeiro State University (UERJ) for their financial support. The authors would also like to thank the LABPETRO - UERJ and CETEM laboratories and their collaborators, for the use of microscopes. The authors are grateful to the Mineral Resources Research Company (CPRM) for providing the geophysical data used in this study

REFERENCES

- Abu El-Ela, F.F., 1996, The petrology of the Abu Zawal gabbroic intrusion, Eastern Desert, Egypt: an example of an island-arc setting: *Journal of African Earth Sciences*, **22**, 2, 147–157. DOI: [10.1016/0899-5362\(96\)00004-8](https://doi.org/10.1016/0899-5362(96)00004-8).
- Almeida, J.C.H., 2000, Zonas de cisalhamento dúctil de alto grau do Médio Vale do Rio Paraíba do Sul: PhD Thesis (in Portuguese), Universidade Estadual Paulista, Rio Claro, SP, Brazil. 190 pp.
- Boyle, R.W., 1982, Geochemical prospecting for thorium and uranium deposits: Elsevier, Netherlands, *Developments in Economic Geology*, **16**, 498 pp.
- Brandalise L.A., C.P. Pinto, H.S. Viana, E.M. Bruno, and M. Zucchetti, 1992, *Província alcalina da Mantiqueira, Serra da Mantiqueira, MG: Revista Escola de Minas (REM)*, **45**, 179–180.
- Brandalise L.A., and H.S. Viana, 1993, Programa de Levantamentos Geológicos Básicos do Brasil, Folha Rio Pomba SF.23-X-D-I. Estado de Minas Gerais: Scale 1:100,000. DNPM/CPRM. Brasília, Brazil. 176 pp.
- Briggs, I.C., 1974, Machine contouring using minimum curvature: *Geophysics*, **39**, 1, 39–48. DOI: [10.1190/1.1440410](https://doi.org/10.1190/1.1440410).
- Bruno, H., V. Elizeu, M. Heilbron, C. de Morisson Valeriano, R. Strachan, M. Fowler, S. Bersan, H. Moreira, I. Dussin, L.G. Eirado Silva, M. Tupinambá, J. Almeida, C. Neto, and C. Storey, 2020, Neoproterozoic and Rhyacian TTG-Sanukitoid suites in the southern São Francisco Palecontinent, Brazil: evidence for diachronous change towards modern tectonics: *Geoscience Frontiers*, **11**, 5, 1763–1787. DOI: [10.1016/j.gsf.2020.01.015](https://doi.org/10.1016/j.gsf.2020.01.015).
- Bruno, H., M. Heilbron, C. de Morisson Valeriano, R. Strachan, M. Fowler, S. Bersan, H. Moreira, R. Motta, J. Almeida, R. Almeida, M. Carvalho, and C. Storey, 2021, Evidence for a complex accretionary history

- preceding the amalgamation of Columbia: the Rhyacian Minas-Bahia Orogen, southern São Francisco Paleocontinent, Brazil: *Gondwana Research*, **92**, 149–171. DOI: [10.1016/j.gr.2020.12.019](https://doi.org/10.1016/j.gr.2020.12.019).
- Carneiro, M.A., and M.S.C. Barbosa, 2008, Implicações geológicas e tectônicas da interpretação magnetométrica da região de Oliveira, Minas Gerais: *Revista Brasileira de Geofísica*, **26**, 1, 87–98. DOI: [10.1590/S0102-261X2008000100007](https://doi.org/10.1590/S0102-261X2008000100007).
- Carrino, T.A., C.R. Souza Filho, and E.P. Leite, 2007, Avaliação do uso de dados aerogeofísicos para mapeamento geológico e prospecção mineral em terrenos intemperizados: o exemplo de Serra Leste, província mineral de Carajás: *Revista Brasileira de Geofísica*, **25**, 3, 307–320. DOI: [10.1590/S0102-261X2007000300007](https://doi.org/10.1590/S0102-261X2007000300007).
- Carvalho, L.M.M., A.C.B. Pires, C.G. Oliveira, R.A.V. Moraes, and M.L.B. Blum, 2006, Processamento e interpretação dos dados magnetométricos aéreos do projeto Itabira-Ferros, MG: uma ferramenta no auxílio ao mapeamento geológico-estrutural: *Revista Brasileira de Geociências*, **36**, Suppl. 1, 85–92. DOI: [10.25249/0375-7536.200636S18592](https://doi.org/10.25249/0375-7536.200636S18592).
- Clark, D.A., 1999, Magnetic petrology of igneous intrusions: Implications for exploration and magnetic interpretation: *Exploration Geophysics*, **30**, 2, 5–26. DOI: [10.1071/EG999005](https://doi.org/10.1071/EG999005).
- Clark, D.A., D.H. French, M.A. Lackie, and P.W. Schmidt, 1992, Magnetic petrology: Application of integrated rock magnetic and petrological techniques to geological interpretation of magnetic surveys: *Exploration Geophysics*, **23**, 1-2, 65–68. DOI: [10.1071/EG992065](https://doi.org/10.1071/EG992065).
- Davis, J.C., 1986, *Statistics and Data Analysis in Geology*, 2nd ed.: John Wiley & Sons, US, 646 pp.
- Dickson, B.L., and K.M. Scott, 1997, Interpretation of aerial gamma-ray surveys – adding the geochemical factors: *AGSO Journal of Australian Geology & Geophysics*, **17**, 2, 187–200.
- Ferraz, A.E.P.P.D., Silva, A., and Ferrari, A.L., 2008, Estudo comparativo entre duas anomalias magnéticas de corpos alcalinos no alto de Cabo Frio e em áreas proximais da Bacia de Santos apoiado por deconvolução de Euler: *Revista Brasileira de Geofísica*, **26**, 4, 469–480. DOI: [10.1590/S0102-261X2008000400007](https://doi.org/10.1590/S0102-261X2008000400007).
- Gaafar, I., 2015, Application of gamma ray spectrometric measurements and VLF-EM data for tracing vein type uranium mineralization, El-Sela area, South Eastern Desert, Egypt: *NRIAG Journal of Astronomy and Geophysics*, **4**, 2, 266–282. DOI: [10.1016/j.nriag.2015.10.001](https://doi.org/10.1016/j.nriag.2015.10.001).
- Guimarães, S.N.P., and V.M. Hamza, 2009, Avanços na caracterização das estruturas Geológicas em subsuperfície da província uranífera Lagoa Real (BA) a partir de dados Aerogeofísicos: *Geosciences = Geociências*, **28**, 3, 273–286. DOI: [10.48550/arXiv.1109.3635](https://doi.org/10.48550/arXiv.1109.3635).
- Gunn, P.J., 1975, Linear transformations of gravity and magnetic fields: *Geophysical Prospecting*, **23**, 2, 300–312. DOI: [10.1111/j.1365-2478.1975.tb01530.x](https://doi.org/10.1111/j.1365-2478.1975.tb01530.x).
- Heilbron, M., W.U. Mohriak, C.M. Valeriano, E.J. Milani, J. Almeida, and M. Tupinambá, 2000, From collision to extension: the roots of the southeastern continental margin of Brazil, in Mohriak, W., and Taiwani, M., eds., *Atlantic Rifts and Continental Margins: Geophysical Monograph Series*, American Geophysical Union, **115**, 1–32. DOI: [10.1029/GM115p0001](https://doi.org/10.1029/GM115p0001).
- Heilbron, M., A.C. Pedrosa-Soares, M.C. Campos Neto, L.C. Silva, R.A.J. Trouw, and V.A. Janasi, 2004, Província Mantiqueira, in Mantesso-Neto, V., A. Bartorelli, C.D.R. Carneiro, B.B. Brito Neves, orgs., *Geologia do continente sul-americano: evolução da obra de Fernando Flávio Marques de Almeida*: Editora Beca, São Paulo, chapter XIII. p. 203–235.
- Hiraga, R., J.R. Nogueira, B.P. Duarte, C.S. Valladares, V.O.M. Guimarães, and R. Peternel, 2017, Geology and Lithochemistry of the Supracrustal Sequence and Interlayered Metabasites of NE Santos Dumont Region (MG). *Anuário do Instituto de Geociências - UFRJ*, **40**, 3, 359–376. DOI: [10.11137/2017_3_359_376](https://doi.org/10.11137/2017_3_359_376).
- Hou, T., Z. Zhang, J. Encarnacion, and M. Santosh, 2012, Petrogenesis and metallogenesis of the Taihe gabbroic intrusion associated with Fe-Ti-oxide ores in the Panxi district, Emeishan Large Igneous Province, southwest China: *Ore Geology Reviews*, **49**, 109–127. DOI: [10.1016/j.oregeorev.2012.09.004](https://doi.org/10.1016/j.oregeorev.2012.09.004).
- IAEA - International Atomic Energy Agency, 1991, Airborne gamma ray spectrometer surveying: Intern. Atomic Energy Agency, Vienna, Technical Reports Series, n° 323. STI/DOC/10/323. 97 pp.
- IAEA - International Atomic Energy Agency, 2003, Guidelines for radioelement mapping using gamma ray spectrometry data: Intern. Atomic Energy Agency, Vienna, IAEA-TECDOC-1363. 173 pp.
- IBGE - Instituto Brasileiro de Geografia e Estatística, 1976, Folha Paiva: IBGE, Diretoria de Geodésia e Cartografia. Rio de Janeiro, 1976. Scale 1:50,000. Carta topográfica. SF-23-X-D-I-3.
- Kärkkäinen, N.K., and T.J. Bornhorst, 2003, The Svecofennian gabbro-hosted Koivusaarenneva magmatic ilmenite deposit, Kälviä, Finland: *Mineralium Deposita*, **38**, 169–184. DOI: [10.1007/s00126-002-0297-0](https://doi.org/10.1007/s00126-002-0297-0).
- Kelley, K.D., C.T. Scott, D.E. Polyak, and B.E. Kimball, 2017, Vanadium, in Schulz, K.J., J.H. DeYoung Jr., R.R. Seal II, and D.C. Bradley, eds., *Critical mineral resources of the United States – Economic and environmental geology and prospects for future supply*: U.S. Geological Survey, Professional Paper 1802, chapter U, Reston, VA, 48 p. DOI: [10.3133/pp1802U](https://doi.org/10.3133/pp1802U).
- Maas, M.V.R., Oliveira, A.C.B., Pires, A.C.B., and Morales, R.A.V., 2003, Aplicação da geofísica aérea

- na exploração mineral e mapeamento geológico do setor sudoeste do Cinturão Cuprífero Orós-Jaguaribe: *Revista Brasileira de Geociências*, **33**, 3, 279–288. DOI: [10.25249/0375-7536.2003333279288](https://doi.org/10.25249/0375-7536.2003333279288).
- Miller, H.G., and V. Singh, 1994, Potential field tilt – a new concept for location of potential field sources: *Journal of Applied Geophysics*, **32**, 213–217. DOI: [10.1016/0926-9851\(94\)90022-1](https://doi.org/10.1016/0926-9851(94)90022-1).
- Minty, B.R.S., 1997, Fundamentals of airborne gamma-ray spectrometry: *AGSO Journal of Australian Geology and Geophysics*, **17**, 39–50.
- Nabighian, M.N., 1972, The analytic signal of two-dimensional magnetic bodies with polygonal cross-section: its properties and use for automated anomaly interpretation: *Geophysics*, **37**, 3, 507–517. DOI: [10.1190/1.1440276](https://doi.org/10.1190/1.1440276).
- Ortiz Suárez, A., A. Morosini, H. Ulacco, and A. Carungo Durán, 2012, *Geología y geofísica del cuerpo máfico-ultramáfico Las Cañas, Provincia de San Luis: Serie Correlación Geológica*, **28**, 2, 151–166.
- Pereira, R. M., M. dos Santos Salomão, R. Neumann, P. Guimarães, and E. Pedroso, 2016, Fe-Ti-V Associado ao Gabro de Lídice, Estado do Rio de Janeiro: *Geonomos*, **24**, 1, 10–20. DOI: [10.18285/geonomos.v24i1.824](https://doi.org/10.18285/geonomos.v24i1.824).
- Pinto, C.P., 1995, *Petrologia de gnaisses alcalinos, cálcio-alcalinos e toleíticas da Serra da Mantiqueira em Minas Gerais – Brasil: Master Dissertation on Geology. Universidade Federal de Minas Gerais, Instituto de Geociências, Belo Horizonte, Brazil.*
- Sarapää, O., N. Kärkkäinen, T. Chernet, J. Lohva, and T. Ahtola, 2005, Exploration results and mineralogical studies on the Lumikangas apatite-ilmenite gabbro, Kauhajoki, Western Finland, *in* Autio, S., ed., *Geological Survey of Finland, GTK, Current Research 2003–2004: Special Paper*, **38**, 31–41. Available on: https://tupa.gtk.fi/julkaisu/specialpaper/sp_038.pdf.
- Sharma, P.V., 1987, Magnetic Method applied to mineral exploration: *Ore Geology Reviews*, **2**, 4, 323–357. DOI: [10.1016/0169-1368\(87\)90010-2](https://doi.org/10.1016/0169-1368(87)90010-2).
- Taylor, S.R., and S.M. McLennan, 1995, The geochemical evolution of the continental crust: *Reviews of Geophysics*, **33**, 2, 241–265. DOI: [10.1029/95RG00262](https://doi.org/10.1029/95RG00262).
- Telford, G., L.P. Geldart, and R.E. Sheriff, 1990, *Applied Geophysics*, 2nd ed., Cambridge University Press, Cambridge, 770 pp.
- Tupinambá, M., M. Heilbron, B.P. Duarte, J.R. Nogueira, C. Valladares, J. Almeida, L.G.E. Silva, S.R. Medeiros, C.G. Almeida, A. Miranda, C.D. Ragatky, J. Mendes and I. Ludka, 2007, *Geologia da Faixa Ribeira Setentrional: estado da arte e conexões com a Faixa Araçuaí: Geonomos*, **15**, 1, 67–79.
- Ulbrich, H.H.G.J., M.N.C. Ulbrich, F.J.F. Ferreira, L.S. Alves, G.B. Guimarães, and A. Fruchting, 2009, Levantamentos gamaespectrométricos em granitos diferenciados. I: revisão da metodologia e do comportamento geoquímico dos elementos K, Th e U: *Revista do Instituto de Geociências - USP*, **9**, 1, 33–53. DOI: [10.5327/Z1519-874X2009000100003](https://doi.org/10.5327/Z1519-874X2009000100003).
- Vaz, O.R.S., M. Salomão, E. Pedroso, R. Pereira, R. Neumann, P. Garcia, and M. Tupinambá, 2017, Magnetita vanadifera do Maciço Ponte Nova: uma Abordagem Exploratória, Vanadiferous magnetite from Ponte Nova Massif and Exploratory Approach: *Anuário do Instituto de Geociências - UFRJ*, **40**, 3, 75–81. DOI [10.11137/2017_3_75_81](https://doi.org/10.11137/2017_3_75_81).
- Viana, H.S., 1991, *Programa Levantamentos Geológicos Básicos do Brasil; carta geológica, carta metalogenética/previsional - Scale 1:100,000 (Folha Barbacena SF.23-X-C-III): DNPM/CPRM, MG, Brazil.*
- Whitehead, N., 2010, *Oasis Montaj 7.2 Viewer: The core software platform for working with large volume spatial data, Tutorials: Geosoft Inc. Toronto, Canada.*
- Wilford, J.R., P.N. Bierwith, and M.A. Craig, 1997, Application of airborne gamma-ray spectrometry in soil/regolith mapping and applied geomorphology: *AGSO Journal of Australian Geology & Geophysics*, **17**, 2, 201–216.
- Zhou, Y., X. Chen, C. Ko, Z. Yang, C. Mouli, and S. Ramanathan, 2013, Voltage-triggered ultrafast phase transition in vanadium dioxide switches: *IEEE Electron Device Letters*, **34**, 2, 220–222. DOI: [10.1109/LED.2012.2229457](https://doi.org/10.1109/LED.2012.2229457).

Dutra, A.C.D.: Main author, study conception and design, data acquisition, result discussion (data analysis and interpretation), manuscript drafting, manuscript critical revision for important intellectual content, version approval of the manuscript to be published, reviews; **Guimarães, S.N.P.:** Study conception and design, result discussion (data analysis and interpretation), manuscript drafting, review interpretation, effective participation in the adequacy of the manuscript through suggestions from the reviewers together with the main author, version approval of the manuscript to be published, reviews; **Salomão, M.S.:** Study conception and design, data acquisition, result discussion (data analysis and interpretation), version approval of the manuscript to be published, reviews; **Palermo, N.:** Study conception and

design, result discussion (data analysis and interpretation), version approval of the manuscript to be published, reviews; **Bertolino, L.C.:** Study conception and design, result discussion (data analysis and interpretation), version approval of the manuscript to be published, reviews; **Bruno, H.:** Study conception and design, result discussion (data analysis and interpretation), version approval of the manuscript to be published, reviews; **Mane, M.A.:** Study conception and design, result discussion (data analysis and interpretation), version approval of the manuscript to be published, reviews.

Received on December 27, 2021 / Accepted on August 09, 2022.

